Pressure-Induced Changes on The Electronic Structure and Electron Topology in the Direct FCC → SH Transformation of Silicon

John S. Tse,[†,*] Michael Hanfland,[‡] Roxana Flacau,[§] Serge Desgreniers,[∥] Zucheng Li,[†] Kolja Mende,[⊥] Keith Gilmore,[‡,¶] Alexander Nyrow,[⊥] Marco Moretti Sala,[‡] and Christian Sternemann[⊥]

[†]Department of Physics and Engineering Physics, University of Saskatchewan, Saskatoon, Saskatchewan S7N 5E2, Canada

[‡]European Synchrotron Radiation Facility, BP 220, F-38047 Grenoble, Cedex, France

[§]Canadian Neutron Beam Center, National Research Council of Canada, Chalk River, Ontario, K0J 1J0 Canada

[∥]Laboratoire de Physique des Solides Denses, Department of Physics, University of Ottawa, Ottawa, Ontario K1N 6N5, Canada

[⊥]Fakultät Physik/DELTA, Technische Universität Dortmund, Maria-Goeppert-Mayer-Strasse 2, D-44221 Dortmund, Germany

[¶]Jiangsu Key Laboratory for Carbon-Based Functional Materials and Devices, Institute of Functional Nano & Soft Materials (FUNSOM), Soochow University, Suzhou, Jiangsu 215123, China

Received: August 29, 2013
Revised: December 18, 2013
Published: December 19, 2013

INTRODUCTION

Through theoretical studies, it is now generally accepted that when an elemental solid is compressed at high pressure in order to alleviate the electron−electron repulsion electrons will leave their bonding configuration and populate the interstitial regions.[1,2] The electron transfer is accomplished by the utilization of more diffuse high-angular momentum atomic orbitals. A well-known example of that interpretation is the case of a structural phase transformation observed in elemental Cs where a 6s → 5d transition occurs, first proposed by Sterheimer.[3] This well-accepted preposition, however, has never been directly verified by experiment. We present experimental evidence with computational support of the electron delocalization in another elemental solid, silicon.

Si has a rich and well-documented high-pressure phase diagram. Under normal conditions, Si adopts face-centered cubic (fcc) structure (Si-I, $Fd\bar{3}m$). When compressed at room temperature, Si first transforms to a β-tin tetragonal structure (Si-II, $I4_1/amd$) at 11 GPa with a large volume reduction;[4] an orthorhombic structure (Si-XI, *Imma*) follows at 13 GPa[5] and a subsequent transformation occurs to a simple hexagonal (sh) phase (Si-V, $P6/mmm$) at 16 GPa.[6,7] Further compression leads to an "open" orthorhombic structure (Si-VI, *Cmca*) at 38 GPa,[8] followed by a hexagonal closed packed structure (hcp, Si-VII, $P6_3/mmc$) at 42 GPa.[7] Dense Si is finally known to further transform to a cubic close-packed fcc structure (Si-X, $Fm3m$) at pressures exceeding 79 GPa.[9] Theoretical electron localization function calculations[7] have shown that the structural transformations in Si are accompanied with a continuous change in the hybridization of Si.[1] It has been advanced that to alleviate the problem of electron repulsion on the atomic sites, the Si 3p-valence electrons are gradually transferred into the more diffuse 3d-orbitals with increasing pressure. For example, semiconducting Si-I becomes metallic in Si-II at 11 GPa. The delocalization of electrons is concomitant with structural transformations: from the ambient three-dimensional (sp^3) covalent bond network in Si-I and Si-II to a two-dimensional (sp^2) planar arrangement in Si-XI, to a one-dimensional (sp) linear network, as observed in Si-V, leading ultimately to a zero-dimensional metal corresponding to Si-VI.[7]

To investigate experimentally the change in hybridization of a compressed solid, the electron density distribution in high-pressure Si was studied with low-temperature powder X-ray diffraction using helium as a quasi-hydrostatic pressure

transmitting medium and the electronic structure was probed X-ray Raman scattering (XRS) spectroscopy.[10] We find that Si−I directly transforms to the sh−Si V phase at 80 K under quasi-hydrostatic conditions and a detailed analysis of the high-pressure X-ray diffraction data by the maximum entropy method (MEM)[11−14] reveals the rehybridization of Si valence bonding orbtials.[1] Modifications of the character of the unoccupied orbitals as a result of the changes in hybridization are directly confirmed by in situ XRS.

EXPERIMENTAL SECTION

Fine Si powder (NIST SRM640c) was loaded together with helium as a pressure transmitting medium into the gasket of a diamond anvil cell (DAC) equipped with 350 μm diameter culet anvils. The gasket material used was hard stainless steel. The cell was placed in a He-flow cryostat and cooled to 80 K. Pressure was determined from the shift of the $^7D_0 - {}^5F_0$ fluorescence line of SrB_4O_7/Sm^{2+} using the calibration of Datchi et al.[15] Powder X-ray diffraction images were recorded on a MAR345 image plate at beamline ID09 at the European Synchrotron Radiation Facility (ESRF) using X-rays with a wavelength of 0.41035 Å. Diffraction images were integrated with FIT2D[15] and the resulting powder diffraction patterns were analyzed by MEM using the RIETAN-2000 software.[12−14] The Debye rings show no azimuthal intensity variations hence the sample was considered free of texture. Rietveld refinements were first carried out on diffraction patterns to extract structure factor of all observed Bragg reflections. The parameters varied during the Rietveld refinements of the diffraction patterns were the scale factor, profile function, background, lattice constants, and the overall thermal parameter. MEM-based pattern fitting (MPF) method implemented in RIETAN-FT[12] was then used to reconstruct the electron density distribution map. MEM calculations were initiated from a uniform prior density distribution by dividing the total number of electrons in the unit cell with a 64 × 64 × 64 pixel mesh. The iterative MEM/MPF procedure was applied until the agreement factor R_I was minimized. Previously the MEM method has been used successfully to extract the valence electron maps of solids under pressure[16−19] and is known to be an efficient technique to minimize artifacts in the electron density map due to truncation errors by the Fourier transform of the experimental structure factors.[11−14,20,21]

High-pressure XRS measurements of elemental Si were performed at beamline ID16 of ESRF with a 30 μm × 120 μm ($v \times h$) beam monochromatized with a Si(111) double crystal and a Si(220) channel cut monochromator. The multianalyzer crystal spectrometer for nonresonant inelastic scattering[22] was used at fixed analyzer energy of 9.69 keV utilizing spherically bent Si(660) crystal analyzers in Rowland geometry. The overall experimental energy resolution was 1 eV. To acquire the Si $L_{II,III}$ edge energy loss spectra the incident energy was scanned at fixed analyzer energy. Analyzed X-rays were detected by a Maxipix 2D detector, which is crucial for separating the signal from background scattering of the sample environment. XRS spectra were measured simultaneously at five different scattering angles between 117 and 143°, resulting in an average momentum transfer of (8.9 ± 0.5) Å^{-1}. From scattering at high momentum transfer, the dipole selection rules are relaxed and nondipolar transitions (p → p) can be probed contributing to the Si XRS spectrum (see refs 23 and 24). Measurements were performed at selected pressures within 3 to 21 GPa at room temperature. Several single spectra were accumulated at each pressure. Because the momentum transfer dependence of the XRS signal at high momentum transfer is weak, spectra obtained for different analyzer crystals were background corrected and summed up yielding the final Si $L_{II/III}$-edge spectrum. The data processing procedure is described in detail elsewhere.[25]

RESULTS AND DISCUSSION

The low-temperature X-ray diffraction patterns measured at 15.9, 17.1, 18.7, and 21 GPa at 80 K are shown in Figure 1.

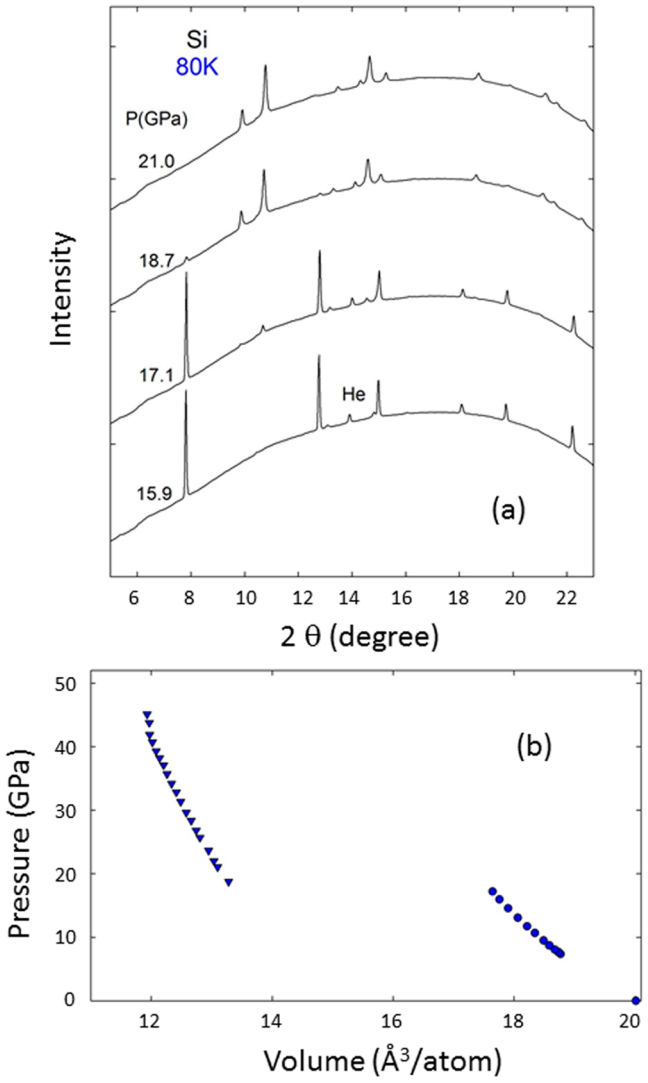

Figure 1. (a) X-ray diffraction patterns of Si recorded at 15.9, 17.1, 18.7, and 21 GPa at 80 K showing the cubic diamond (Si-I) to primitive hexagonal phase (Si-V) transition. (b) Pressure volume relation of Si at 80 K.

With Si compressed at 80 K, we observed the persistence of an X- ray diffraction pattern corresponding to the diamond structure of Si-I up to around 17 GPa (Figure 1a). An abrupt structural transition to the sh Si-V was observed upon compression above 17 GPa (Figure 1b) with no indication of the intermediate Si−II (β-tin) and Si-XI (orthorhombic) phases. Results of MEM analyses for X-ray diffraction patterns recorded at 14.5, 15.9, and 21 GPa are summarized in Figure 2a−c. Comparisons of the theoretical[26−31] and derived structure factors for the first eight Bragg peaks used in the

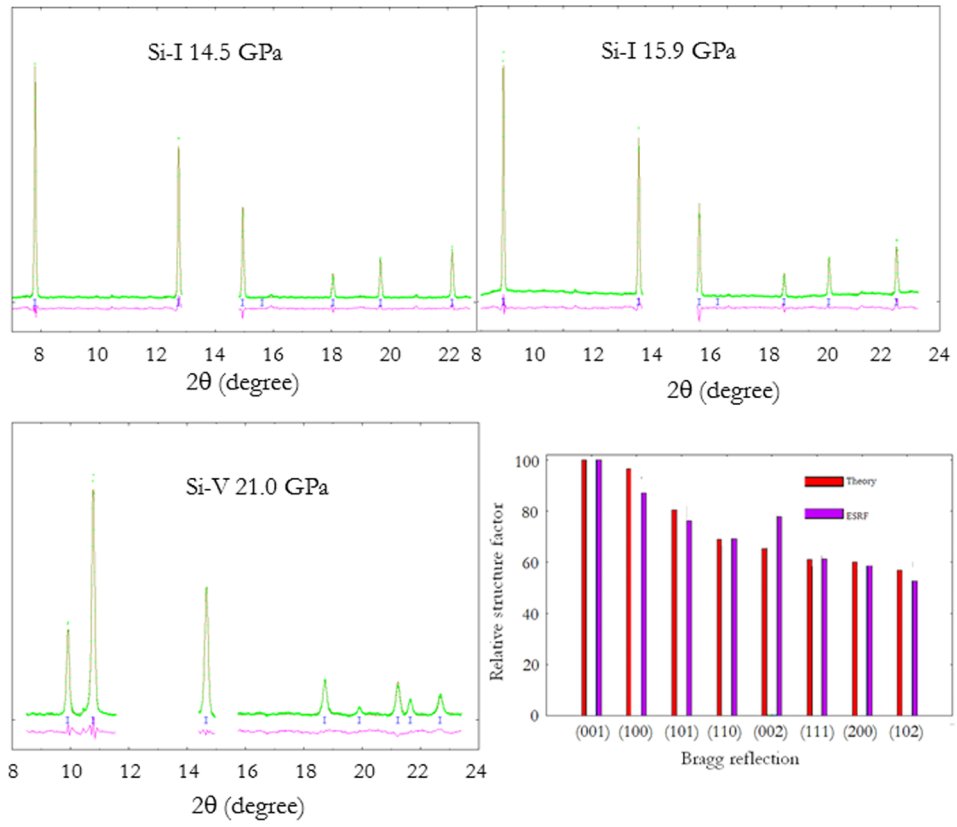

Figure 2. Comparison of experimental and MEM/MPF fitted powder X-ray diffraction of Si at (a) 14.5, (b) 15.9, and (c) 21 GPa. (d) Comparison of measured and calculated structure factors of the Bragg reflections used in the MEM analysis of Si-V. Theoretical structure factors for Si-V were computed using the CRYSTAL09 code[27] using a double-ζ plus polarization (6-21G*) basis set[28] employing the Perdew–Burke–Ernzerhof hybrid density functional (PBE0).[29] Theoretical structure factors were corrected for temperature effect using the experimental thermal parameter determined from Rietveld refinement. Theoretical electron densities were calculated with the Vienna Ab initio Simulation Package (VASP)[30] employing a plane wave basis set and the projected augmented wave (PAW) potential.[31]

MEM analysis of the Si-V phase at 21 GPa and relative to the (001) reflection are presented in Figure 2d. In this case, the agreement between theory and experiment is indeed excellent and can be certainly considered within the error of the measurement. The only exception is the (002) reflection where the extracted structure factor is 15% too high. Therefore, it is possible to extract reliable structure factors from MEM-optimized Rietveld refinements of the experimental powder X-ray diffraction patterns utilizing only a limited number of low angle Bragg reflections, because the atomic form factors can be separated into core and valence electron contribution and the latter is dominating for low angles due to the larger radii of the valence electron orbitals. A MEM analysis using these structure factors is capable to describe the change of the electron topology between the Si-I and Si-V phases, adopting the diamond and sh structures, respectively.

The corresponding electron density distribution maps determined by MEM analyses are shown in Figure 3. For the Si–I phase, the presence of covalent Si–Si bonds is evident from the increase of electron density between Si atom pairs along the [011] plane.[32] By comparing the electron density distribution of the Si–Si bonds at 14.5 and 15.9 GPa (Figure 3a,b), the electron density distribution clearly becomes more diffuse and disperse away from the bond axes. This observation is consistent with an increased participation of diffuse Si 3d orbitals in the chemical bonding. The electron topology in the Si-V phase (sh) at 21 GPa differs significantly from that of the Si-I phase (Figure 3c). The most dramatic change, shown in the

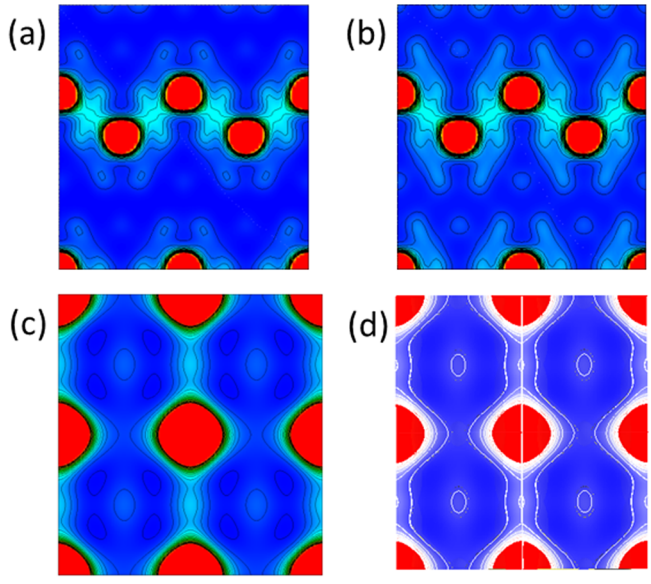

Figure 3. Electron density maps in the [011] plane of Si-I obtained from the MEM analysis of the corresponding X-ray diffraction pattern measured at 14.5 (a) and 15.9 GPa (b). The electron density distribution map in the [010] plane of Si-V measured at 21 GPa (c) is compared to the theoretical charge density (d). The contour lines are from 0 to 2 e/Å^3 at intervals of 0.1e/Å^3.

[010] plane, is in fact the absence of electron density between Si atoms within the hexagonal layers in which the Si−Si contact distance is the shortest. On the contrary, electrons are found to concentrate between Si atoms between layers aligned along the crystallographic *c*-axis. Moreover, pockets of enhanced electron density are found located at the interstitial sites. This observation of charge delocalization is in complete agreement with previous theoretical predictions.[2] In fact, the calculated electron density associated with the Si-V phase, plotted along the [010] plane, is in semiquantitative agreement with the experimental density obtained from MEM analyses as shown in Figure 3d. The result is striking as a very limited number of low-angle Bragg reflections, eight in this case, have been used to reconstruct the electron density distribution map. An extended X-ray diffraction pattern, not possible given our experimental geometry limiting the accessible reciprocal space, would have most likely given a better agreement between the experimental and theoretical results.

To further investigate the changes in the electronic structure due to orbital rehybridization, XRS measurements in the vicinity of the Si $L_{II,III}$-edge (2p) were performed and compared with ab initio calculations. Si powder together with a small piece of ruby was loaded into a panoramic DAC[33,34] without pressure transmission medium using a beryllium gasket. The pressure was measured by the ruby fluorescence method before and after spectra were acquired. The experimental XRS spectra of the Si $L_{II/III}$-edge at different pressures are shown in Figure 4

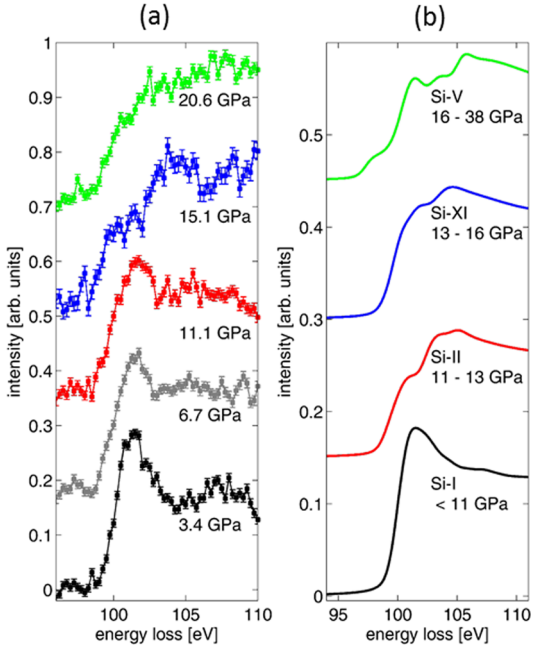

Figure 4. (a) XRS spectra of pure silicon taken at different pressures. (b) Calculations of XRS spectra for different silicon phases corresponding to conditions at which the experimental data was taken (see text for details).

in the left panel. The spectrum recorded at 3.44 GPa is very similar to that reported at ambient pressure.[23,24] The most pronounced peak at 101.5 eV is due to strong core-hole interactions (excitonic excitation) and is a characteristic feature of the semiconducting behavior of the material.[23] It can be assigned mainly to transitions to the dipole allowed p → s and d channels.[24] The shape of the spectrum for energy losses above 102.5 eV is dominated by monopole transitions to p-like final states. As can be seen, the spectra at 6.7 and 11.1 GPa already show a decrease of the main absorption peak which is accompanied by peak broadening. The change in the main absorption peak indicates increasing metallicity and the broadening points to increasing disorder of the system approaching the phase transition from Si−I to Si−II. However, we cannot exclude broadening due to the pressure gradient in the absence of a hydrostatic medium. At 15.1 GPa significant changes in the overall spectral shape are observed despite the marginal quality of the spectrum measured in the intermediate phase. The intensity of the dominant 2p → s and d transitions is strongly reduced and the overall spectrum is characterized by a smoothly rising intensity. This observation is clearly confirmed by the spectrum of Si-V taken at 20.6 GPa. The loss of the main absorption peak, characteristic for the semiconductor Si-I phase, is indicative of the transformation to a state with increasing metallicity.

Calculations of the XRS spectra using the Bethe-Salpeter Equation (BSE) method were performed with the OCEAN code (obtaining core-level excitations using ab initio methods and the NIST BSE solver).[35,36] The calculated XRS spectra were convoluted with the experimental resolution of 1 eV. The results are compared with the observed spectra in Figure 4, right panel. The trends in the calculated spectra are in good agreement with the experimental data (Figure 4, left). With increasing pressure the main absorption peak is strongly reduced changing from Si-I to Si-II and spectral weight is transferred to energy losses above 102.5 eV. The smooth increase in overall shape of XRS spectra for pressures above 11 GPa is in accordance with the experiment. More detailed information is obtained by inspection of the DOS (see Figure SI (Supporting Information)).[36] The DOS transforms from semiconducting to free electron-like. This clearly reveals the rising metallicity of the system with increasing pressure. Both sets of calculations indicate a complete change in the system's properties occur by the first phase transition from Si-I to Si-II. As commented above, the contribution of Si 3d electrons to unoccupied states in the metallic phase becomes progressively more pronounced as pressure increases. Thus, the width of Si 3d band is spread over a broader energy range and accompanied by a broadening of the unoccupied s states close to the Fermi level resulting in a reduction of the intensity of the main 2p → d, s transition.

CONCLUSIONS

Experimental and computational evidence demonstrating s, p → d rehybridization accompanying the insulator → metal transition in elemental Si were presented. High-resolution powder X-ray diffraction, obtained using synchrotron radiation, demonstrates the vital role of using a hydrostatic pressure transmitting medium and temperature in the study of structural phase transitions. The observation the direct transformation from the diamond to the sh structure of Si at low temperature bypassing the intermediate Si−II and Si-XI phases suggests the respective transition activation barriers may be too high to be surpassed at low temperatures. A direct diamond → sh transition has been predicted in a variable cell constant-pressure ab inito molecular dynamics calculation[37] under nonequilibrium conditions when the pressure was raised from 0 to 30 GPa at 300 K instantaneously. In contrast, a subsequent study employing a meta-dynamics scheme,[38] which allows exploration of the potential energy surface, recovered the

observed room temperature diamond → tetragonal → orthorhombic → sh transformation sequence. The theoretical results are consistent with the present study. At low temperature, the small thermal activation energy does not allow the sampling of all possible transformation pathways and the phase transition is kinetically controlled. The mechanism leading to the change in the electron topology from the Si-I to the Si-V phases reported here is consistent with a previous MEM analysis of pressure-induced isostructural transition in the Ba_8Si_{46} clathrate.[17] In the earlier work, the phase transition of Ba_8Si_{46} was also found to occur close to 17 GPa and the chemical bonding revealed from the electron density maps shows the change from s−p to s−p−d hybridization.[2,18] The common transition pressure of 17 GPa in pure silicon and in Ba_8Si_{46} may not be coincidence but a strong indication that a change in hybridization will always occur whenever a Si framework is compressed to this critical pressure (hence density). In both cases, Si and Ba_8Si_{46}, mixings of Si valence 3sp states with diffuse 3d orbitals help to alleviate the repulsive interactions between electrons in the Si−Si bonding region allowing the electron delocalization into the interstitial region. The metallization due to orbital rehybridization is confirmed by XRS measurements in combination with ab initio calculations. In passing, it is noteworthy that elemental Ge also has a fairly complicated high pressure phase diagram where several stable or metastable structure may coexist in the same pressure range.[39]

ASSOCIATED CONTENT

Supporting Information

Details on the Bethe-Salpeter Equation calculations of the Si *L*-edge X-ray Raman spectra are described and the calculated density of states of the high pressure polymorphs of silicon is shown. Figure showing the density of states of the high-pressure polymorphs of silicon. This material is available free of charge Internet.

AUTHOR INFORMATION

Corresponding Author

*E-mail: John.Tse@usask.ca. Tel.: +1 306-966-6410.

Notes

The authors declare no competing financial interest.

ACKNOWLEDGMENTS

We kindly acknowledge ESRF for providing synchrotron radiation. We would like to thank J. J. Rehr, M. Tolan, Ch. J. Sahle, and J. A. Soininen for discussions and support. T. Brenner and L. Simonelli are acknowledged for help with the XRS measurements. The BSE calculations were performed on the Nano and Vulcan computer clusters of the Molecular Foundry at Lawrence Berkeley National Lab, which is supported by the Office of Science, Office of Basic Energy Sciences, of the U.S. Department of Energy. Financial support was given by BMBF (05K10PEC) and DOE (DE-FG03-97ER45623) . K.G. has been supported by the National Natural Science Foundation of China (Grant 11375127) and the Natural Science Foundation of Jiangsu Province (Grant BK20130280) and in part by DOE BES grant DE-FG03-97ER45623. Part of the calculations was performed at the Westgrid Computing Cluster through a grant to JST.

REFERENCES

(1) Tse, J. S. In *Modern Charge-density Analysis*; Gatti, C., Macchi, P., Eds.; Springer Verlag: New York, 2012.

(2) Tse, J. S. Crystallography of High Pressure Elemental Solids. *Z. Kristallogr.* **2006**, *220*, 521−530.

(3) Sternheimer, R. M. On the Compressibility of Metallic Cesium. *Phys. Rev.* **1950**, *78*, 235−243.

(4) Jamieson, J. C. Crystal Structures at High Pressures of Metallic Modifications of Silicon and Germanium. *Science* **1963**, *139*, 762−764.

(5) McMahon, M. I.; Nelmes, R. J. New High-pressure Phase of Si. *Phys. Rev. B* **1993**, *47*, 8337−8340.

(6) Olijnyk, H.; Sakka, S. K.; Holzapfel, W. B. Structural Phase transitions in Si and Ge Under Pressures Up To 50 GPa. *Phys. Lett.* **1984**, *103A*, 137−140.

(7) Hu, J. Z.; Spain, I. L. Phases of Silicon at High Pressure. *Solid State Commun.* **1984**, *51*, 263−266.

(8) Hanfland, M.; Schwarz, U.; Syassen, K.; Takemura, K. Crystal Structure of the High-Pressure Phase Silicon VI. *Phys. Rev. Lett.* **1999**, *82*, 1197−1200.

(9) Duclos, S. J.; Vohra, Y. K.; Ruoff, A. L. hcp to fcc Transition in Silicon at 78 GPa and Studies to 100 GPa. *Phys. Rev. Lett.* **1987**, *58*, 775−779.

(10) Schülke; W. *Electron Dynamics by Inelastic X-Ray Scattering*, Oxford University Press: Oxford, 2007.

(11) Sakata, M.; Sakata, M. The Principle of the Maximum Entropy Method. *High Press. Res.* **1996**, *14*, 327−333.

(12) Izumi, F.; Kumazawa, S.; Ikeda, T.; Hu, W. Z.; Yamamoto, A.; Oikawa, K. MEM-based Structure-refinement System REMEDY and its Applications. *Mater. Sci. Forum* **2000**, *378−3*, 59−64.

(13) Izumi, F.; Dilanian, R. A. *Recent Research Developments in Physics*, Part II; Transworld Research Network: Trivandrum, India, 2002; Vol. 3, pp 699−726.

(14) Momma, K.; Ikeda, T.; Belik, A. A.; Izumi, F.; Dysnomia, A. Computer Program for Maximum-entropy method (MEM) Analysis and its Performance in the MEM-based Pattern Fitting. *Powder Diffr.* **2013**, *28*, 184−193.

(15) Datchi, F.; LeToullec, R.; Loubeyre, P. Improved Calibration of the SrB_4O_7:Sm^{2+} Optical Pressure Gauge: Advantages at Very High Pressures and High Temperatures. *J. Appl. Phys.* **1997**, *81*, 3333−3339.

(16) Hammersley, A. P.; Svensson, S. O.; Hanfland, M.; Fitch, A. N.; Häusermann, D. Two-dimensional Detector Software: From Real Detector to Idealised Image or Two-theta Scan. *High. Pres. Res.* **1996**, *14*, 235−248.

(17) Fujihisa, H.; Fujii, Y.; Takemura, K.; Shimomura, O.; Nelmes, R. J.; McMahon, M. I. Pressure Dependence of the Electron Density in Solid Iodine by the Maximum-Entropy Method. *High Press. Res.* **1996**, *14*, 335−340.

(18) Tse, J. S.; Flacau, R.; Desgreniers, S.; Jiang, J. Z. Electron Density Topology of High-pressure Ba_8Si_{46} from a Combined Rietveld and Maximum-entropy Analysis. *Phys. Rev. B* **2007**, *76*, 174109.

(19) Flacau, R.; Tse, J. S.; Desgreniers, S. Electron Density Topology of Cubic Structure I Xe Clathrate Hydrate at High Pressure. *J. Chem. Phys.* **2008**, *129*, 244507.

(20) Tse, J. S. *Chemical Applications of Synchrotron Radiation*; Sham, T. K., Ed.; World Scientific: Singapore, 2002.

(21) Sakata, M.; Itsubo, T.; Nishibori, E.; Moritomo, Y.; Kojima, N.; Ohishi, Y.; Takata, M. Charge Density Study Under High Pressure. *J. Phys. Chem. Solids* **2004**, *65*, 1973−1976.

(22) Verbeni, R.; Pylkkänen, T.; Huotari, S.; Simonelli, L.; Vankó, G.; Martel, K.; Henriquet, C.; Monaco, G. Multiple-element Spectrometer for Non-resonant Inelastic X-ray Spectroscopy of Electronic Excitations. *J. Synch. Radiat.* **2009**, *16*, 469−475.

(23) Sternemann, H.; Soininen, J. A.; Sternemann, C.; Hämäläinen, K.; Tolan, M. Near-edge Structure of Non-resonant Inelastic X-ray Scattering from *L*-shell Core Levels Studied by a Real-space Multiple-scattering Approach. *Phys. Rev. B* **2007**, *75*, 075118.

(24) Sternemann, C.; Soininen, J. A.; Huotari, S.; Vankó, G.; Volmer, M.; Secco, R. A.; Tse, J. S.; Tolan, M. X-ray Raman Scattering at the *L*

edges of Elemental Na, Si, and the *N* Edge of Ba in Ba_8Si_{46}. *Phys. Rev. B* **2005**, *72*, 035104.
(25) Sternemann, H.; C. Sternemann, C.; Seidler, G. T.; Fister, T.; Sakko, A.; Tolan, M. An Extraction Algorithm for Core-level Excitations in Non-resonant Inelastic X-ray Scattering Spectra. *J. Synch. Radiat.* **2008**, *15*, 162−169.
(26) Dovesi, R.; Orlando, R.; Civalleri, B.; Roetti, C.; Saunders, V. R.; Zicovich-Wilson, C. M. CRYSTAL: A Computational Tool for the Ab Initio Study of the Electronic Properties of Crystals. *Z. Kristallogr.* **2005**, *220*, 571−573.
(27) Dovesi, R.; Saunders, V. R.; Roetti, C.; Orlando, R.;. Zicovich-Wilson, C. M.; Pascale, F.; Civalleri, B.; Doll, K.; Harrison, N. M.; Bush, I. J.; D'Arco, Ph.; Lunell, L. *CRYSTAL09 User's Manual*; University of Torino: Torino, 2009.
(28) Hehre, W. J.; Radom, L.; Schleyer, P. V.; Pople, J. A. *Ab inito Molecular Orbital Theory*; Wiley-Interscience: New York, 1986.
(29) Adamo, C.; Barone, V. Toward Reliable Density Functional Methods Without Adjustable Parameters: The PBE0Model. *J. Chem. Phys.* **1999**, *110*, 6158−6170.
(30) Kresse, G.; Furthmüller, J. Efficiency of Ab-initio Total Energy Calculations for Metals and Semiconductors Using a Plane-wave Basis Set. *Comput. Mater. Sci.* **1996**, *6*, 15−50.
(31) Kresse, G.; Joubert, D. From Ultrasoft Pseudopotentials to the Projector Augmented-wave Method. *Phys. Rev. B* **1998**, *59*, 1758−1775.
(32) Sakata, M.; Sato, M. Accurate Structure Analysis by the Maximum-Entropy Method. *Acta Crystallogr., Sect. A* **1990**, *46*, 263−270.
(33) R. Lübbers, R.; Grünsteudel, H. F.; Chumakov, A. I.; Wortmann, G. Density of Phonon States in Iron at High Pressure. *Science* **2000**, *287*, 1250−1253.
(34) Giefers, H.; Lübbers, R.; Grünsteudel, H. F.; Chumakov, A. I.; Wortmann, G. Phonon Density of States in Orientated hcp Iron by Nuclear Inelastic Scattering of Synchrotron Radiation. *High Press. Res.* **2002**, *22*, 501−506.
(35) Vinson, J.; Rehr, J. J.; Kas, J. J.; Shirley, E. L. Bethe-Salpeter Equation Calculations of Core Excitation Spectra. *Phys. Rev. B* **2011**, *83*, 115106.
(36) Detail information on the BSE calculations and the calculated density of states are provided in the Supporting Information.
(37) Focher, P.; Chiarotti, G. L.; Bernasconi, M.; Tosatti, E.; Parrinello, M. Structural Phase Transformations via First-Principles Simulation. *Europhys. Lett.* **1994**, *26*, 345−352.
(38) Behler, J.; Martonak, R.; Donaldio, D.; Parrinello, M. Metadynamics Simulations of the High-Pressure Phases of Silicon Employing a High-Dimensional Neural Network Potential. *Phys. Rev. Lett.* **2008**, *100*, 185501.
(39) Cui, H. B.; Graf, D.; Brooks, J. S.; Kobayashi, H. Pressure-Dependent Metallic and Superconducting Phases in a Germanium Artificial Metal. *Phys. Rev. Lett.* **2009**, *102*, 237001.